SPE-175014-MS

Society of Petroleum Engineers

# New Rock-Typing Index Based on Hydraulic and Electric Tortuosity Data for Multi-Scale Dynamic Characterization of Complex Carbonate Reservoirs

Ferreira, F.C., Booth, R., Oliveira, R., SPE, Schlumberger, Carneiro, G., Bize-Forest, N., and Wahanik, H., Schlumberger



This paper was prepared for presentation at the SPE Annual Technical Conference and Exhibition held in Houston, Texas, USA, 28–30 September 2015.



## Abstract

Rock-pore-space geometry and network topology have a great impact on dynamic reservoir characteristics, in particular on capillary pressure and relative permeability curves. Hydraulic tortuosity is a key independent measurement relating the pore-space geometry and topology to the rock's effective porosity and absolute permeability. Therefore, hydraulic tortuosity can be an important concept for dynamic reservoir characterization and reservoir simulation. Our objectives are to recommend a new dynamic rock-typing process and to assess the corresponding improvement on reservoir simulation processes.

We introduce an innovative dynamic reservoir-rock-typing (DRRT) index, using absolute permeability, porosity and hydraulic tortuosity data, derived from mercury-injection capillary pressure (MICP) experiments. For correlation purposes, we also derived electric tortuosity data from formation-resistivity experiments. We used the experimental data from the Worldwide Rock Catalog (WWRC) provided by a joint-industry project (Core Lab, 2014), for both carbonate and clastic rocks. Based on the new proposed DRRT index and on corresponding dynamic reservoir properties, we prepared a comprehensive sensitivity study on the impact of hydraulic tortuosity variability on oil recovery results. This sensitivity study was done by incorporating the concept of hydraulic tortuosity in a synthetic carbonate-reservoir simulation model.

The analysis of the MICP and formation-resistivity data showed both greater average tortuosity and greater tortuosity variability for carbonates, when compared with clastic rocks. It also showed good correlation between hydraulic and electric tortuosity values. The sensitivity study results showed a significant impact of hydraulic tortuosity variability on oil in place and reserves estimates for improved oil recovery (IOR) / enhanced oil recovery (EOR) processes in typical complex carbonate reservoirs, such as the ones found in the Brazilian Pre-Salt. It also showed the importance of applying proper corrections while deriving dynamic reservoir properties from capillary pressure and relative permeability experiments.

The new DRRT index shows a much stronger correlation with pore-space geometry when compared with traditional reservoir-quality (RQI) and flow-zone (FZI) indexes. Therefore, it has clear potential to

enhance the dynamic rock-typing process for reservoir simulation of IOR / EOR in complex carbonate rocks. We also discuss the importance of an integrated laboratory test and well log program to enable the proper upscaling and geostatistical distribution of dynamic rock properties.

In complex carbonate reservoirs under IOR / EOR, overlooking the rock-pore-space geometry and network topology may result in significant errors in reservoir characterization and simulation processes. In this context, proper DRRT in carbonates, including tortuosity, is therefore crucial for reservoir simulation; enabling correspondence between core, well log and reservoir-scale dynamic properties. The presented correlation between hydraulic and electric tortuosity significantly increases the potential of dielectric measurements for dynamic reservoir characterization of complex carbonates on both core and well log scales.

## Introduction

Accurate static and dynamic reservoir characterization are key requirements for reservoir management and simulation. The characterization workflows rely on the integration of data and understanding across multiple scales and domains - from the pore scale to the reservoir scale and through the petrophysics, reservoir engineering, geology and geophysics domains. Reservoir characterization methodologies estimate rock properties from core, well log and seismic measurements, and then distribute such properties throughout the reservoir by associating geological facies to petrophysical facies, and identifying static and dynamic reservoir-rock types (Cosentino, 1992; Jerry Lucia, 1999). Several methodologies classify reservoir-rock types by rock-typing-index ranges (e.g. Winland $R_{35}$, RQI or FZI - Amaefule et al., 1993; Stolz and Graves, 2003). These rock-typing indexes seek to describe a relationship between the effective porosity $\phi_e$, representing the storage capacity of the reservoir, and the absolute permeability $k$, representing the reservoir flow capacity. The reservoir-quality index (RQI) is defined by:

$$\mathrm{RQI} = \sqrt{k/\phi_e}, \tag{1}$$

while the flow-zone indicator (FZI) is defined by:

$$\mathrm{FZI} = \mathrm{RQI}/\phi_z, \tag{2}$$

where $\phi_z$ is the normalized porosity, given by:

$$\phi_z = \phi_e/(1-\phi_e). \tag{3}$$

Winland (see Pitman, 1992) has defined the $R_{35}$ index from MICP experiments as the pore-throat radius corresponding to the capillary pressure at 35% of mercury saturation. He has correlated such index to absolute permeability and effective porosity by:

$$\log(R_{35}) = a\log(k) - b\log(\phi_e) + c, \tag{4}$$

where *a*, *b* and *c* are constants which may be adjusted to a specific formation.

The above reservoir-rock-typing indexes describe relationships between the effective porosity and the absolute permeability, which are both very important reservoir properties. For a number of processes (e.g. pressure transient; and fractional flow at reservoir-layer scale), $\phi_e$ and $k$ may even fully characterize the

reservoir response. Nevertheless, for multiphase transport in porous media, a more complete dynamic reservoir characterization may be required and this is the focus of this study. The main corresponding capillary effects are wettability; capillary pressure and relative permeability curves; end-point saturations; and hysteresis. Such capillary effects are especially important for the simulation of reservoirs under IOR / EOR processes, or producing under gas or water natural drives.

We may better understand such phenomena by thinking of a fluid particle inside a pore. It can only interact with other nearby fluid particles and with the pore walls. From this pore-scale perspective, one cannot derive bulk properties like absolute permeability and effective porosity. The consequences are clear by examining the Young-Laplace-Washburn (1921) equation for the drainage capillary pressure $P_c$:

$$P_{\mathrm{c}} = \frac{2\gamma\cos(\theta)}{r_{\mathrm{throat}}}. \tag{5}$$

In the above equation, the fluids' interfacial tension $\gamma$ represents the fluid-fluid interactions, the contact angle $\theta$ represents the fluid-rock interactions, and the pore-throat radius $r_{\mathrm{throat}}$ represents the pore space geometry. There is no direct reference to either absolute permeability or effective porosity. Therefore, pore-scale properties rule the capillary effects. Relevant pore-scale geometry properties include pore-body and pore-throat sizes; percolation path and threshold; pore connectivity and pore shape. Rock mineralogy, fluid characteristics, and their interactions under reservoir conditions complete the required data scenario for a proper dynamic characterization. Such pore-scale property distributions are difficult to obtain in the laboratory, virtually impossible from well logs. Therefore, which bulk properties may help us better infer the pore-scale properties? To find out, we examine the following modified Kozeny equation (see Appendix A):

$$\langle r_{\mathrm{throat}}^2 \rangle = 8\frac{k\tau_h}{\phi_e}, \tag{6}$$

where $\tau_h$ is the hydraulic tortuosity and $\langle r_{\mathrm{throat}}^2 \rangle$ is the average pore-throat squared radius. Therefore, hydraulic tortuosity $\tau_h$ measurements may enhance the dynamic reservoir characterization, linking absolute permeability and effective porosity to pore-space geometry, and connecting the pore and the core scales.

We then compare Eqs. (1), (2), (4) and (6). Eq. (6) shows that rocks with the same ratio $k/\phi_e$ may have very different pore-throat sizes, if the hydraulic tortuosity $\tau_h$ is different from rock to rock. The RQI formulation (Eq. (1)) implicitly considers $\tau_h$ to be nearly constant. This may be a reasonable assumption for most clastic rocks. However, in the more complex carbonate rocks, RQI may not properly represent the pore-space properties. In FZI equation (2), the normalized porosity $\phi_z$ may partially account for the hydraulic tortuosity $\tau_h$, in the case of rocks with round-shaped grains with low to moderate diagenesis (see Appendix A). We regard the $R_{35}$ index (from MICP) as a closer representation of the pore space characteristics when compared with RQI and FZI. Nevertheless, Winland $R_{35}$ equation (4) may only properly represent the $R_{35}$ index from MICP when the hydraulic tortuosity $\tau_h$ is constant or shows some correlation with $k$ and $\phi_e$. When tortuosity variability is high, we may then consider $\tau_h$ an independent variable, so we expect the Winland $R_{35}$ index to show a poor regression coefficient with respect to the $R_{35}$ index from MICP. In such cases, the resulting poor correlation will adversely affect the $R_{35}$ index upscaling to the wellbore and reservoir scales.

Therefore, RQI, FZI and Winland $R_{35}$ indexes have limited applicability, especially when dealing with complex reservoir rocks such as the Pre-Salt mixed-wet carbonates in Brazil, with planned CO2 injection

/ WAG processes (Pizarro and Branco, 2012). Indeed, microbial and travertine fabrics dominate the Pre-Salt carbonate rocks in Brazil and show a high degree of vertical and horizontal heterogeneity resulting from their genesis and diagenesis processes. Matrix dissolution, which creates vugs, and geothermal cementation that closes the pore space, have a large impact on the tortuosity of the resulting macro and meso-pore systems, in addition to their corresponding absolute permeability.

To better characterize the more complex carbonate-reservoir rocks and identify the corresponding DRRT, Stolz and Graves (2003) also included MICP data as a secondary grouping strategy for dynamic reservoir-rock-typing indexes. T2 distributions from nuclear magnetic resonance (NMR) well logs can be used as a proxy for MICP pore-throat-size distributions (Kleinberg, 1996), but effects such as body-to-throat-size ratio (BTR), varying surface relaxivity and wettability can impact the accuracy of this method, making it difficult to upscale the DRRT based only on NMR logs.

We would ideally include the hydraulic tortuosity as an independent reservoir property to allow better static and dynamic reservoir characterization of complex reservoirs, especially when producing under IOR / EOR processes, or under gas or water natural drives.

Nooruddin et al. (2011) had also recognized the limitations of RQI and FZI for carbonate rocks. To overcome such limitations, they proposed a new approach starting from FZI equation (2) and the Kozeny-Carman (K-C) equation:

$$k = \left(\frac{1}{f_g \tau_{kc} S_{Vgr}^2}\right) \phi_e \, \phi_z^2, \tag{7}$$

where $f_g$ is the shape factor, $\tau_{kc}$ is the K-C tortuosity and $S_{Vgr}$ is the specific surface area of the grain.

They combined the above equation with the electric tortuosity $\tau_e$ equation:

$$\tau_e = \left(\frac{a}{\phi^{(m-1)}}\right)^2, \tag{8}$$

where $\phi$ is the total porosity, $a$ is the tortuosity factor and $m$ is the cementation exponent from the Archie's equation. Using the above equation and considering the tortuosity factor $a = 1$, they replaced the K-C tortuosity $\tau_{kc}$ in Eq. (7) with the electric tortuosity $\tau_e$ calculated from the cementation exponent $m$. They then proposed a modified flow-zone indicator $\mathrm{FZI_m}$:

$$\mathrm{FZI_m} = \mathrm{RQI} \Big/ (\phi_z \times \phi^{(m-1)}). \tag{9}$$

The above equation complements the normalized porosity $\phi_z$ in the FZI formulation, which partially accounts for the hydraulic tortuosity $\tau_h$. Although the definitions of the K-C tortuosity $\tau_{kc}$ and the electric tortuosity $\tau_e$ are not identical (see Appendix A), Nooruddin et al. (2011) reported promising results for some Middle-East carbonate rocks.

Any dynamic reservoir characterization methodology is incomplete if laboratory core measurements cannot be upscaled to the wellbore and reservoir scales. For example, current rock-typing indexes use effective porosity and absolute permeability. Porosity measurements from well logs are relatively straightforward. On the other hand, absolute permeability upscaling requires correlations with effective porosity and other well logs, like the nuclear magnetic resonance (NMR) log. Specific correlations and

neural-network techniques may replace missing measurements to some extent. Therefore, we should also identify well log measurements and techniques, which enable the upscaling of hydraulic tortuosity.

An improved reservoir characterization model should make uncertainties explicit even when the data or good correlations for replacing such data are unavailable. Explicit uncertainties, such as the hydraulic tortuosity in complex carbonates, will drive the improvement of reservoir data acquisition and analysis. However, the acquisition and processing of new special core analysis (SCAL) and well log data are expensive. Therefore, to justify the additional costs, we should clearly demonstrate the benefit corresponding to reduced uncertainty in the estimation of hydraulic tortuosity.

In this study, we propose a new dynamic reservoir-rock-typing index ( $RQI^*$) using absolute permeability, porosity and hydraulic tortuosity data, derived from MICP experiments. We analyzed the MICP and formation-resistivity data from the WWRC. The data show both greater average tortuosity and greater tortuosity variability for carbonates, when compared with clastic rocks. The $RQI^*$ shows a much stronger correlation with pore-space key parameters when compared with traditional RQI and FZI indexes, especially for carbonates. Therefore, $RQI^*$ is a better guide for the distribution of capillary pressure and relative permeability curves, with a clear potential to enhance the reservoir simulation of IOR / EOR in complex carbonate rocks, at both history matching and production forecast phases.

We also derive electric tortuosity data from formation-resistivity experiments. The data show good correlation between hydraulic and electric tortuosity values. Multi-frequency dielectric measurements (in both core and well log scales) may also provide the cementation exponent and the corresponding electric tortuosity estimates. Such combination of core and well log analysis may enable the upscaling of hydraulic tortuosity and $RQI^*$, as well as the proper distribution of capillary pressure and relative permeability curves.

Based on the new index $RQI^*$, on the modified $J^*$-function introduced by El-Khatib (1995), and on corresponding dynamic reservoir properties, we prepare a comprehensive sensitivity study on the impact of hydraulic tortuosity variability on oil recovery results, using a synthetic carbonate-reservoir simulation model. The sensitivity study results show a significant impact of hydraulic tortuosity variability on oil-in-place and reserves estimates for improved oil recovery (IOR) / enhanced oil recovery (EOR) processes in typical complex carbonate reservoirs, such as the ones found in the Brazilian Pre-Salt. The sensitivity study also shows the importance of applying proper corrections while deriving dynamic reservoir properties from capillary pressure and relative permeability experiments.

## New Dynamic Rock-Typing Index Based on Hydraulic Tortuosity

Based on the modified Kozeny equation (6) we propose a new index for dynamic reservoir-rock typing:

$$RQI^* = \sqrt{k\tau_h/\phi_e} = \sqrt{\langle r_{throat}^2 \rangle/8}\,. \tag{10}$$

The definition above highlights the direct correlation between $RQI^*$ and the rock-pore-throat-size distribution. Therefore, we expect that it may significantly improve dynamic reservoir characterization and capillary effects upscaling for reservoir simulation.

Using a similar approach, El-Khatib proposed a modified $J^*$-function (see Appendix A):

$$J^*(S_w^*) = \frac{P_c}{\gamma \cos(\theta)} \sqrt{\frac{k\tau_h}{\phi_e}} = \frac{2}{r_{\text{throat}}} \sqrt{\frac{k\tau_h}{\phi_e}} = \frac{2\text{RQI}^*}{r_{\text{throat}}}, \tag{11}$$

which is directly proportional to the ratio between $\text{RQI}^*$ and the corresponding $r_{\text{throat}}$. By knowing $\text{RQI}^*$, we may then obtain drainage capillary pressure curves combining Eq. (11) to the distribution of $r_{\text{throat}}$ as a function of the normalized wetting-fluid saturation $S_{\text{w}}^*$:

$$S_{\text{w}}^* = \frac{(1 - S_{\text{w}})}{(1 - S_{\text{wmin}})}, \tag{12}$$

where $S_{\text{wmin}}$ is the minimum wetting-fluid saturation.

## Data Setup

We use the WWRC data to estimate the hydraulic and electric tortuosity values and analyze several possible correlations within the data. This catalog is the result of a joint-industry project. It comprises 155 carbonate and clastic samples from around the world. We selected 41 out of 49 carbonate samples for our present study. The samples are classified according to geological and petrophysical indexes, allowing the analysis of rock-property correlations for specific facies. We use data from routine core analysis, steady state mercury-injection capillary pressure (MICP) and resistivity-formation-factor (RFF) experiments. Gas absolute permeability is corrected according to Klinkenberg (1941). With a few exceptions, the different experiments were run on the same core plugs, increasing the likelihood of correlation between different derived properties.

MICP and RFF experiments are relatively cheap and precise. They have progressively become more important in carbonate reservoir characterization. Therefore, we believe there is a large potential for future application of this study results to other carbonate fields.

We numerically integrate the integral form of Eq. (6) to calculate the hydraulic tortuosity from the MICP data:

$$\tau_h = \frac{\phi_e}{8k} \int_0^1 r_{\text{throat}}^2 . \, dS_{\text{Hg}}^* \, . \tag{13}$$

We propose the following workflow:

- Remove any eventual residual Hg dead volume;
- Calculate the pore-throat equivalent radius for each capillary pressure step, using Eq. (5);
- Calculate the normalized mercury-saturation difference $\Delta S_{\text{Hg}}^*$ for each pressure step;
- Calculate incremental hydraulic tortuosity contribution $\Delta\tau_h$;
- Determine maximal pore-throat radius $R_d$ corresponding to the capillary entry pressure $P_d$ where mercury saturation starts to increase;
- Determine $R_{35} = r_{\text{throat}}$ at $S_{\text{Hg}} = 35\%$;
- Calculate hydraulic tortuosity $\tau_h$;
- Calculate average pore-throat squared radius $\langle r_{\text{throat}}^2 \rangle$;
- Calculate the rock-typing indexes: RQI, FZI, FZIm, Winland R35 and RQI$*$.

From Eq. (13), $\tau_h$ mostly depends on the squared radii of the larger pore throats. We need a good characterization of this pore-throat-size range during the MICP experiment. It may therefore require low-pressure range MICP and accurate dead volume corrections. We also recommend avoiding the use of capillary pressure fitting models as they may misrepresent the actual low-pressure MICP data. Modern MICP experiments already provide very good pore-throat-distribution characterization in the low-pressure range. MICP experiments are cheap, fast and precise. MICP experiments present no wettability issues, are consistent with gas corrected permeability, cover a large pressure range and usually result in very low residual-air saturation.

## Hydraulic Tortuosity Distribution Results

**Figure 1** shows the hydraulic-tortuosity probability distribution for the WWRC carbonate rocks. It also shows the tortuosity distribution for limestones and dolostones. For the whole set of samples, we find a large variability consistent with the complexity of their genesis and diagenesis: $\tau_h$ ranges from 2 to almost 300, with a mean value of $\langle \tau_h \rangle = 32$, and a standard deviation of $\sigma(\tau_h) = 55$. As expected, the hydraulic tortuosity distribution best fits a lognormal distribution.

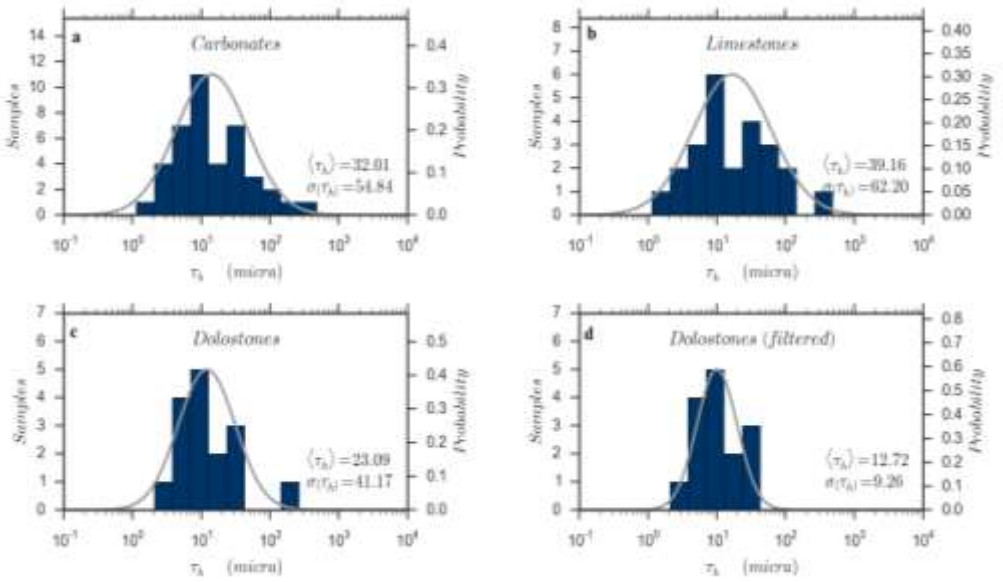


*Figure 1 - WWRC hydraulic tortuosity probabilistic distribution for (a) carbonates, (b) limestones, (c) dolostones and (d) dolostones excluding the highest tortuosity value. The horizontal axes of the histograms are logarithmic.*

Dolostones (**Figure 1c**) show significantly smaller mean value and standard deviation of hydraulic tortuosity, particularly when excluding the outlier corresponding to the highest tortuosity sample (**Figure 1d**). Conversely, limestone rocks show a high mean value and standard deviation (**Figure 1b**). Bize-Forest et. al. (2014) analyzed the correlation between the cementation exponent $m$ and porosity $\phi_e$ for the same WWRC carbonates. They explained the relationship between $m$ and tortuosity, and the reasons why different genesis and diagenesis processes result in different quality rocks with different tortuosity values.

For example, in the case of limestones with interparticle porosity (not shown in Figure 1), the tortuosity mean value of $\langle \tau_h \rangle = 28$ and the standard deviation of $\sigma(\tau_h) = 38$ are smaller than those observed for other limestone samples. The dolostone samples present a good rock quality and a low tortuosity mean value, similar to those found in clastic rocks, except for one vuggy sample with a very high tortuosity. Regardless of the differences in the results between the subsets of samples, the standard deviation value is similar to, or higher than the mean value, which is a good indication of high tortuosity variability and corresponding reservoir heterogeneity.

## Comparison between RQI* and other Rock-Typing Indexes

**Figure 2** shows a log-log plot of RQI versus the hydraulic tortuosity $\tau_h$ (x-axis is reversed), for the WWRC carbonates. The colored sloping lines correspond to equally spaced RQI* values. Such plot is very similar to the standard plot of RQI versus the normalized porosity $\phi_z$, with lines corresponding to the FZI values. The reason is clear when we look at the following equations:

$$\mathrm{FZI} = {\mathrm{RQI}}/{\phi_z} \tag{2}$$

$$\mathrm{RQI}^* = \mathrm{RQI}\sqrt{\tau_h} \tag{14}$$

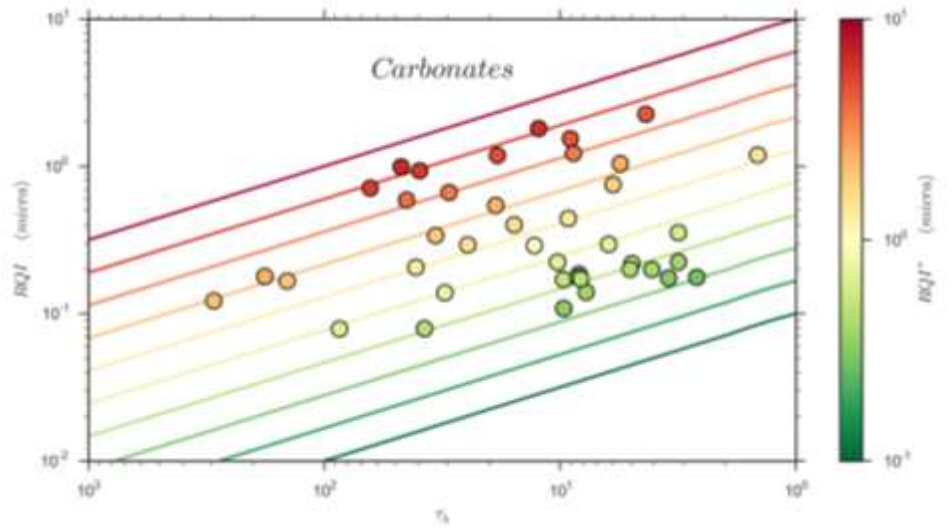


*Figure 2 - RQI vs Hydraulic Tortuosity vs RQI* plot for the WWRC Carbonates – similar to usual FZI plot*

Usually, as first proposed by Amaefule et al. (1993), the points in the plot should correspond to identified hydraulic flow units (HFU). However, it can be used for any parameter we might wish to compare against the RQI* lines. Unfortunately, the concept of HFU is not applicable to a worldwide catalog data. We instead plan to apply this approach to a future field study.

The similarities between FZI and RQI* equations show that $\phi_z$ partially accounts for $\tau_h$, due to the supporting assumptions of the K-C equation (7), which are only true for rocks formed by round-shaped grains or particles, with low to moderate diagenesis impact. We believe RQI* covers all FZI cases, being superior to FZI for complex carbonate rocks. On the other hand, clastic rocks may show better correlation

of hydraulic tortuosity with porosity $\phi_e$, absolute permeability $k$ and RQI than carbonates. When this is the case, it is a good indication that an empirical and field-specific correlation between effective porosity and absolute permeability could partially replace the need for an independent tortuosity measurement. However, complex carbonate rocks show a lack of such correlation between hydraulic tortuosity and effective porosity, absolute permeability or RQI, suggesting that hydraulic tortuosity should be considered an independent parameter for such rocks. Such an indication has led us to propose the new rock-typing index RQI*.

In the industry, $R_{35}$ and $R_d$ are considered key points for drainage capillary pressure curve characterization. They are also relevant key points for relative permeability and end-point saturations. $R_d$ is the pore-throat size corresponding to the entry capillary pressure, the highest pressure before the non-wetting fluid first enters the rock. $R_{35}$ corresponds to the capillary pressure when the non-wetting-fluid saturation reaches 35%. **Figure 3** shows the position of such points on a capillary pressure curve. $R_{35}$ and $R_d$ may be calculated using Eq. (5).

For unimodal pore-throat-size rocks, such key points may be enough for a good capillary pressure curve characterization. In the case of multimodal rocks, like most carbonates, $R_{35}$ and $R_d$ are usually associated with the larger-pore system. In addition, relative permeability curves are mostly defined by the larger-pore system. Therefore, multimodal pore-throat-size distribution analysis is then required to complement the characterization of the smaller-pore system.

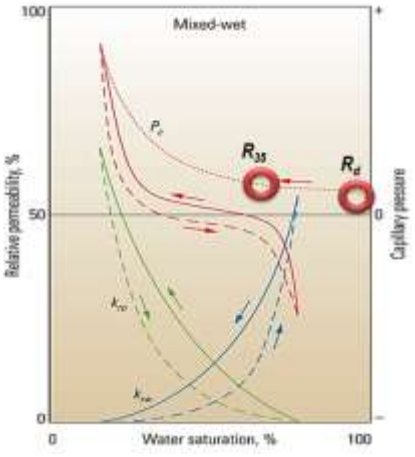


*Figure 3 - Drainage capillary pressure key points (modified over the original picture from Schlumberger Oilfield Review, Summer 2007, pg. 50)*

Besides the most used rock-typing indexes, we also considered the $FZI_m$ index, as proposed by Nooruddin et al. (2011). We share their vision in which the electric tortuosity $\tau_e$ derived from the cementation exponent $m$ may help us to infer the hydraulic tortuosity $\tau_h$. However, because $\tau_e$ and $\tau_h$ are similar but different concepts (Clenell, 1997), we believe that the best approach is to keep both concepts separated and assess the quality of their correlation.

**Figure 4** shows plots for correlations between $R_{35}$ and rock-typing indexes RQI*, Winland $R_{35}$, RQI, FZI and $FZI_m$. $R_d$ correlations are also shown on the right side of Figure 4.

RQI* shows excellent near-linear correlation with both $R_{35}$ and $R_d$, whereas Winland $R_{35}$, RQI, FZI and $FZI_m$ all show a fair correlation with $R_{35}$, but a poor correlation with $R_d$. Considering that the 41 carbonate samples in the WWRC come from around the world, we may expect RQI* correlations to improve in the case of a specific field, reservoir, formation and facies. Moreover, the dolostones in the WWRC do not show a large tortuosity variability. Consequently, we expect the comparison between RQI* and the other indexes to further improve as the tortuosity variability of a specific dataset increases.

Most of the WWRC carbonate samples show a bimodal pore-throat-size distribution. Nevertheless, RQI* still presents excellent correlation with $R_{35}$ and $R_d$.

Therefore, the proposed rock-typing index RQI* is a significant improvement for reservoir dynamic characterization, particularly for complex rocks.

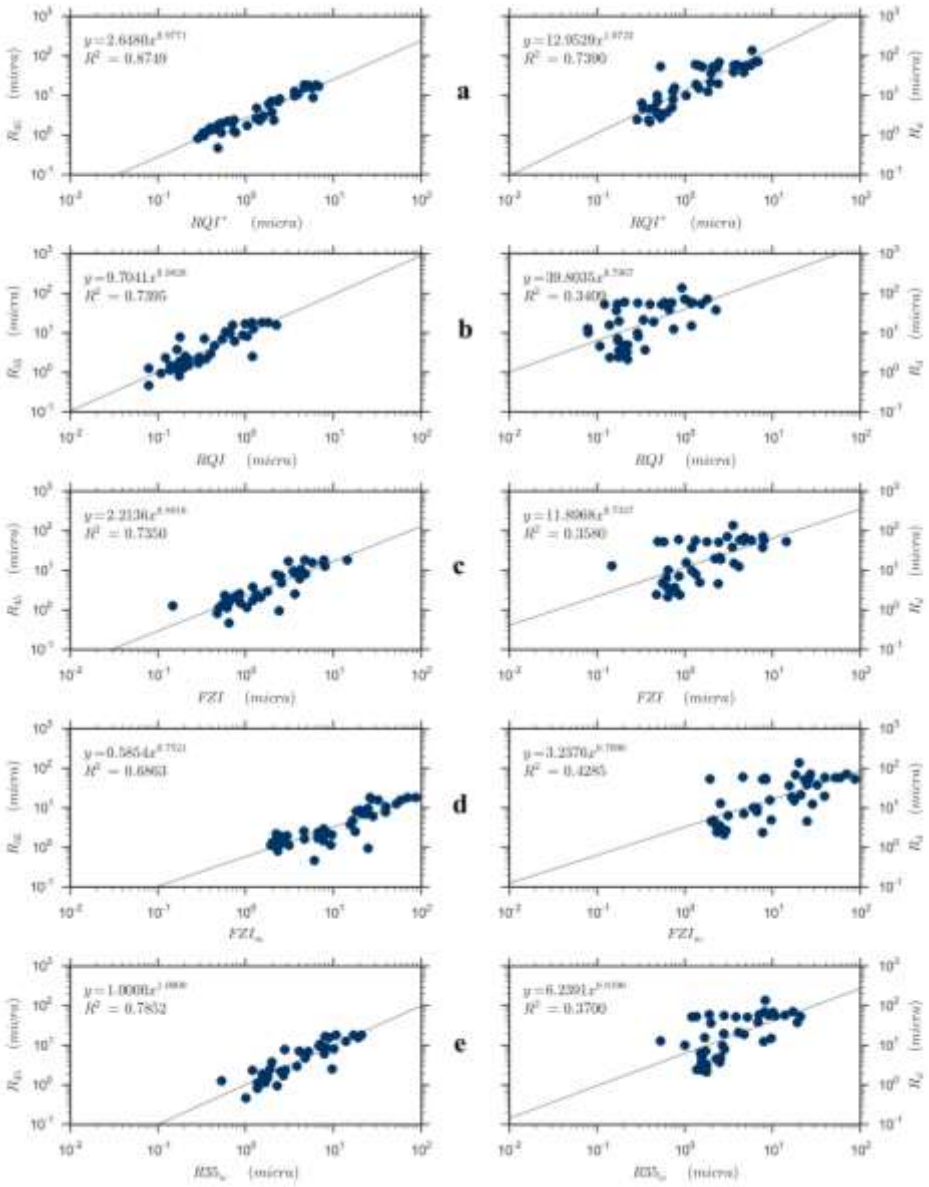


*Figure 4- $R_{35}$ correlations (on the left side) with (a) RQI*, (b) RQI, (c) FZI, (d) $FZI_m$ and (e) Winland $R_{35}$. $R_d$ corresponding correlations are shown on the right side.*

## Hydraulic and Electric Tortuosity Correlation

We obtain the cementation exponent $m$ and the tortuosity factor $a$ from the RFF experiments run in the same 41 carbonate samples from the WWRC. We then calculate the electric tortuosity $\tau_e$ using Eq. (8).

**Figure 5** shows the correlation between hydraulic tortuosity $\tau_h$ and the electric tortuosity $\tau_e$ for the WWRC carbonates. Despite the fact that the samples come from around the world with very different characteristics, we find a good correlation between electric and hydraulic tortuosity for both carbonate and clastic rocks. The correlation improves when we select specific characteristics, as for the limestone carbonates with interparticle porosity.

The red lines in the plots show the identity line. In the vast majority of the cases, the electric tortuosity is significantly greater than the hydraulic tortuosity. Nevertheless, on average, the relationship between the two parameters is close to a linear function, another indication of good correlation. Electric and hydraulic tortuosities are similar physical concepts but should show different values. They present several similarities. They include the percolation-path ratio (geometric tortuosity) effect. As the absolute permeability, these tortuosities are also anisotropic properties, depending on the direction of measurement. Both may also depend, although in different ways, on body-to-throat-size ratio (BTR); rock lamination; clay content; pore-geometry type and network connectivity. Both equations, relating electric and hydraulic potential with their corresponding flow in porous media, include pore-size power-law terms. However, they also present significant differences: different physical phenomena and corresponding equations; different methods for measurement; different wettability environments; different sensitivity to clay content.

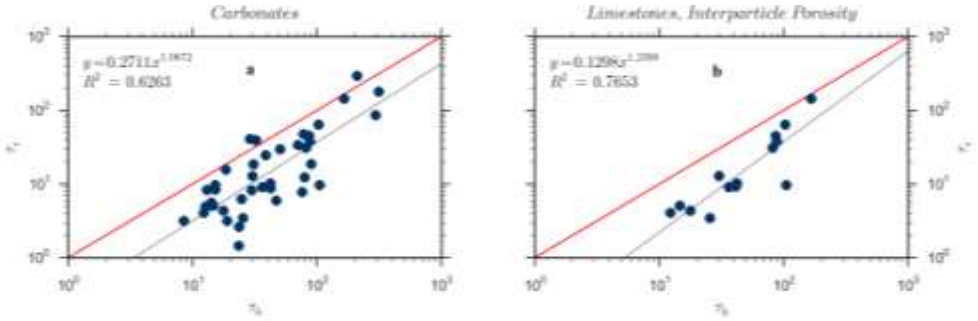


*Figure 5 - Hydraulic and electric tortuosity correlation for:*
*(a) WWRC carbonates and (b) WWRC limestones with interparticle porosity*

The correlation between electric and hydraulic tortuosity usually improves when the type of rock, grain size, clay content and porosity type are similar. Therefore, we expect that the correlation between electric and hydraulic tortuosity to be stronger for samples belonging to the same field, same formation, and same geological facies with the same clay content.

The good correlation between hydraulic tortuosity $\tau_h$ and the electric tortuosity $\tau_e$ significantly increases the potential of using well logs to upscale both properties.

## Dielectric Measurements for Tortuosity Upscaling

Dielectric measurements measure effective formation permittivity and conductivity. Permittivity is the medium's ability to resist an external electric field and is related to electric susceptibility, which measures the degree of polarization in response to the electric field. Because water is more polarizable than oil, it presents much higher values for permittivity. Such characteristic makes it possible to calculate water-filled porosity from dielectric data. Modern, multi-frequency dielectric-logging tools use mixing interpretation models for fitting effective permittivity to dispersion data (Seleznev, 2006) and provide textural information such as the Archie's cementation exponent $m$. With $m$ determined, and considering an estimate for the tortuosity factor $a$, it is then possible to calculate the electric tortuosity $\tau_e$ using Eq. (8), enabling the upscale of the hydraulic tortuosity $\tau_h$ if a suitable correlation exists between the two properties. Laboratory dielectric measurements may support and further develop the current interpretation models.

Because dielectric measurements improve the accuracy of water-saturation estimates, the uncertainty in the reservoir saturation-height model (SHM) may be reduced. A good SHM combined with a better dynamic rock typing may result in more reliable estimates for hydrocarbon volumes in place and recovery.

## Reservoir Simulation and Hydraulic Tortuosity

To our knowledge, commercial reservoir simulation software does not directly support a hydraulic tortuosity parameter, nor the El-Khatib $J^*$-function. However, we employ a suitable workaround, by coherently changing both the permeability and the transmissibility multipliers, in order to allow the Leverett $J$-function (1941) to perfectly simulate the El-Khatib $J^*$-function, while preserving the model transmissibility.

We also replace RQI with RQI* to map the corresponding rock types to the simulator rock regions. The following equations summarize the workaround:

$$\mathrm{RQI}^* = \mathrm{RQI}\,\sqrt{\tau_h}\,, \tag{14}$$

$$J^*(S_w^*) = J(S_w^*)\,\sqrt{\tau_h}\,, \tag{15}$$

$$k^* = k\,\tau_h\,, \tag{16}$$

$$T_M^* \cong {T_M}/{\tau_h}\,, \tag{17}$$

where in fact the modified transmissibility multiplier $T_M^*$ calculation depends on the specific transmissibility calculation algorithm used by the simulator software. Permeability is a tensor property. Therefore, $\tau_h$ and $T_M^*$ are also tensor properties. However, $k^*$is a scalar property (see Eq. (6)).

Where the rock type changes across a grid cell boundary due to a change in the cell tortuosity value, we use the following dynamic characterization and simulation strategies to smooth the transition of the capillary effects. Leverett $J$-function curves, derived from typical pore-throat-size distributions compatible with each rock type, are used to scale the capillary pressure according to the ratio between absolute permeability and effective porosity. We also employ a two-point end-point-scaling for both capillary pressure and relative permeability curves. Such smoothing strategies eliminate any effects of discontinuities in the simulation model, so that the impact of the tortuosity variability is physical.

## Tortuosity Uncertainty Impact on Oil-in-Place and Reserves Estimates

### Proposed Workflow

The balance between the corresponding benefits and costs determines the value of a dynamic reservoir characterization process. Acquiring and analyzing data from cores, well logs, well tests and other surveys set the costs. The resulting decreased reservoir characterization uncertainties defines the benefits. A sensitivity analysis of the impact of the reservoir uncertainties over the field economics quantifies such benefits. Hydraulic tortuosity variability may affect both absolute permeability and capillary effects uncertainties. In this study, we focus on the impact of tortuosity variability on capillary effects, i.e. capillary pressure and relative permeability curves. We do not consider any impact on the absolute permeability.

**Figure 6** shows the workflow for such an impact assessment. If representative MICP data are available, the first step (a) is to analyze the statistical distribution of the derived hydraulic tortuosity. If the results show a large variability in tortuosity (quantified by the standard deviation) compared with the mean tortuosity value, we then proceed to the next step, otherwise there is no significant impact. The current and future types of reservoir-energy sources define the importance of capillary effects for the economic results. Reservoirs developed under natural solution gas or compaction drives are not significantly impacted. In contrast, results from reservoirs developed under IOR / EOR, natural gas or water drives are very responsive to capillary pressure effects. The next step (b) is to build a reservoir model with several stochastic realizations of the tortuosity distribution and the corresponding capillary pressure and relative permeability curves. A sector model or a semi-synthetic reservoir model may be used to avoid excessive computation time, if it is representative of the reservoir behavior. In step (c), we then consider two main impacts of tortuosity variability on dynamic characterization: the fluid-saturation distribution in the transition zone, influenced by capillary pressure curves; and the decrease of displacement-fluid sweep efficiency due to fingering and channeling, mainly influenced by relative permeability curves, saturation end-points, rock heterogeneity and fluid-mobility ratio ($M$). In step (d), after putting together the sensitivity analysis results, we then review our reservoir data acquisition and characterization processes.

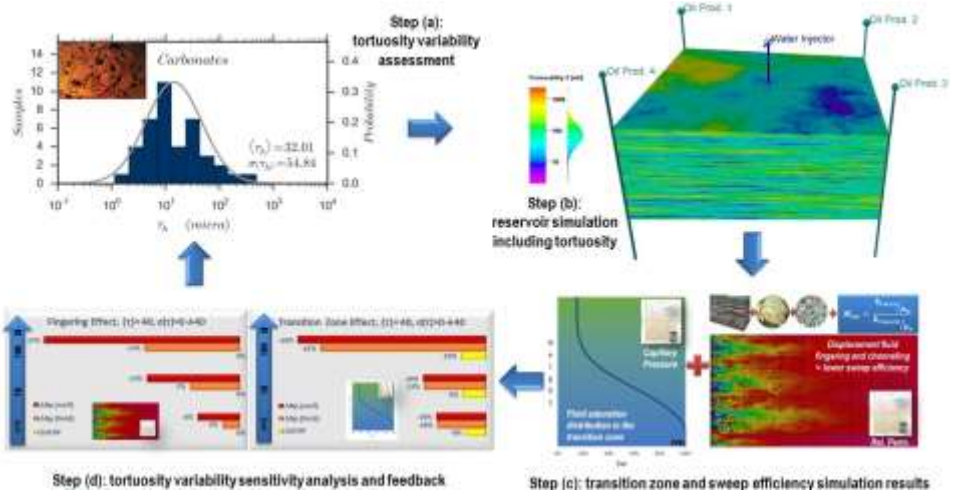


*Figure 6- Workflow for assessment of impact of tortuosity variability*

## Synthetic Simulation Model

For the purpose of this study, we set a synthetic carbonate-reservoir simulation model comprising an inverted five-spot pattern for water injection into the oil zone, as illustrated in **Figure 6b**.

We build a regular Cartesian fine grid, with 50 x 50 x 100 layers and 250,000 active cells, to model a 500 x 500 x 100 ft pattern. We set the well completions according to a standard strategy: the injection well is perforated over the bottom 50 ft and the four producer wells are all perforated over the top 30 ft of the reservoir thickness. Therefore, water may flow upwards, probably improving the oil sweep efficiency.

The impact assessment considers the effects of the change in tortuosity distribution over the reservoir original oil in place, oil recovery factor and oil ultimate recovery, as well as the changes in the heterogeneous dynamic behavior at the well's level.

We distribute the reservoir properties throughout the fine model grid using sequential Gaussian simulation (SGS). Such distributions are set considering a specific degree of reservoir heterogeneity.

We also set three different mobility-ratio cases: light, average and heavy oil, where oil densities and viscosities were set according to typical industry ranges. Under water injection, such cases approximately correspond to mobility ratios of 1, 10 and 100.

An overly complex reservoir model could hinder the assessment of the tortuosity impact over capillary effects. Therefore, we employ some simplifying assumptions. The water-injection voidage-replacement fraction is equal to one, i.e. almost all produced liquids are replaced by injection, maintaining the reservoir pressure close to its initial value. We use simple but realistic well operation constraints: bottom-hole pressure and water-cut limits. An oil-water model is set, i.e. no free gas, while keeping the reservoir pressure way above the bubble pressure. The reservoir rock is moderately water-wet reservoir, with no hysteresis and no fractures, and presents a single lognormal pore-throat-size distribution.

We create the base case by distributing the effective porosity, RQI and the absolute permeability tensor through SGS. We then define rock types based on RQI ranges. We also use the RQI values to estimate the end-point saturation and maximum relative permeability values for each grid cell, using typical monotonic correlations. We use a similar approach to estimate the Corey's exponents for relative permeability.

Using the reservoir-tortuosity mean value $\langle \tau_h \rangle$, we also create an equivalent correlation between the end-points and RQI* defined by Eq. (10). Combining the El-Khatib $J^*$ Eq. (11), truncated lognormal pore-throat-size distribution and the mean tortuosity value, we create an equivalent Leverett $J$-function curve for each rock type (see also Eq. (15)), consistent with the RQI and RQI* corresponding ranges. We set the free-water level (FWL) 15 ft below the depth of the model-grid base to obtain a significant transition-zone thickness when compared to the total grid thickness.

We then validate the simulation base case for general consistency, comparing the corresponding oil recovery results for the different mobility ratios.

Afterwards, we set a validation case by introducing the hydraulic tortuosity concept in the reservoir simulation model. We initialize the validation-case model by setting, for the whole grid, a constant hydraulic tortuosity property equal to the reservoir-tortuosity mean value $\langle \tau_h \rangle$. We then run the validation case and compare the corresponding results with the base-case results, which does not include the

tortuosity concept or the workaround. We expect an exact match of the results in both reservoir and well scales.

Finally, we create multiple simulation cases to investigate the sensitivity to hydraulic tortuosity. For this analysis, we keep all spatial property distributions fixed, except for the hydraulic tortuosity. We make no other changes to the simulation model. We create the multiple sensitivity cases by altering the distribution of the hydraulic tortuosity, keeping the hydraulic tortuosity mean value $\langle \tau_h \rangle$ fixed and only varying the standard deviation $\sigma(\tau_h)$. Several stochastic realizations of the tortuosity are required for each case of the sensitivity analysis. By using the above workaround, RQI* cell values change with the hydraulic tortuosity distribution, increasing the heterogeneity of capillary effects. The corresponding rock regions, the capillary pressure and relative permeability curves, and the end-point scale properties change according as RQI* changes. The match of the simulation results to the base-case results improves continuously as we decrease the standard deviation of the hydraulic tortuosity $\sigma(\tau_h)$.

At last, if the tortuosity variability is high, the core sampling for the capillary pressure and relative permeability experiments may unintentionally miss the mean value of the hydraulic tortuosity $\langle \tau_h \rangle$. Therefore, if no corrections are made, such experimental results are defined by the actual hydraulic tortuosity of the samples, and do not represent the average capillary behavior for the corresponding rock types. To assess the corresponding impact, we run separate sensitivity cases, varying the mean value of the hydraulic tortuosity $\langle \tau_h \rangle$ while keeping the standard deviation $\sigma(\tau_h)$ equal to zero.

## Hydraulic Tortuosity Sensitivity Data

Data for the complex Pre-Salt limestone rocks in Brazil are not presently available for this tortuosity sensitivity study. Therefore, we choose to model a synthetic, porous, permeable, moderately complex carbonate reservoir.

Because of the worldwide nature of the WWRC, we cannot consider the tortuosity data distribution for the WWRC limestone as a complete analog for the Pre-Salt-rock tortuosity. Using the same tortuosity mean value may be a good guess, but the standard deviation of a specific Pre-Salt-rock type may be smaller than the WWRC limestone standard deviation. On the other hand, the Pre-Salt rock may be more complex than most of the WWRC limestones. As a result, we choose to set a hydraulic tortuosity mean value of $\langle \tau_h \rangle = 40$ and consider a range of tortuosity standard deviation from $\sigma(\tau_h) = 0$ to a maximum of $\sigma(\tau_h) = 40$. Any greater values for $\langle \tau_h \rangle$ and $\sigma(\tau_h)$ would lead to greater sensitivity impacts.

Table 1 shows the parameters and strategies to distribute the synthetic reservoir properties throughout the simulation model grid.

*Table 1 - Sensitivity Study Property Distribution*

| Property | Type | Mean | Std. Dev. |
|---|---|---|---|
| Effective Porosity $\phi_e$ | *Normal* | 20% | 3.5% |
| RQI | *Lognormal* | 0.6 | 0.3 |
| Absolute Permeability ($k_x = k_y$) | $k_{x,y} = RQI^2.\phi_e$ | 96 mD | 96 mD |
| $k_z/k_x$ | *Normal* | 0.3 | 0.1 |
| Absolute Permeability ($k_z$) | $k_z = k_z/k_x \,.\, k_x$ | 29 mD | 33 mD |
| Hydraulic Tortuosity ($\tau_x = \tau_y$) | *Lognormal* | 40 | {0,4,10,40} |
| Hydraulic Tortuosity ($\tau_z$) | $\tau_z = \tau_x.k_x/k_z$ | (150-175) | (400-1000) |

To populate the grid with the static properties, we use a sequential Gaussian simulation with a fixed spherical variogram using distances of 250 ft, 250 ft and 2 ft, resulting in facies layers with approximately ¼ of the five-spot area and as thin as 2 ft, as shown in Figure 6. We distribute the effective porosity according to a normal (Gaussian) distribution. To distribute the absolute horizontal permeability ($k_x = k_y$), we use a RQI lognormal distribution to result in a lognormal permeability distribution, correlated with porosity. To obtain the vertical absolute permeability ($k_z$), we use a normal distribution of the vertical to horizontal permeability ratio, and then use this property to distribute the vertical permeability. We keep the same effective porosity, absolute permeability and RQI distributions for all the simulation cases. We start by using both horizontal hydraulic tortuosity distribution ($\tau_x = \tau_y$) with a mean value $\langle\tau_h\rangle = 40$ and a standard deviation $\sigma(\tau_h) = 40$. We then progressively reduce the standard deviation $\sigma(\tau_h)$ to 10, 4 and then 0 to allow us to assess the sensitivity to tortuosity variability. We then calculate the vertical tortuosity ($\tau_z$) based on the horizontal tortuosity and the vertical to horizontal permeability ratio ($k_z/k_x$).

We set three separate synthetic fluid models to use as alternatives in the sensitivity cases, shown in Table 2. The corresponding oil viscosities present an approximated ratio of 1:10:100, allowing for very different mobility ratios to be tested.

*Table 2 - Fluid Properties for the Sensitivity Study*

| Fluid Properties | API | Psat (psia) | Boi @ 5000 psia | μoi (cP) | Rsi (scf/stb) |
|---|---|---|---|---|---|
| Light Oil | 35 | 2500 | 1.275 | 0.66 | 568 |
| Average Oil | 20 | 1500 | 1.103 | 5.2 | 183 |
| Heavy Oil | 15 | 1000 | 1.088 | 71.25 | 92 |

## Hydraulic Tortuosity Variability Sensitivity Results

**Figure 7** shows one sample of the several results for the tortuosity variability sensitivity. It shows the reservoir results for the average-oil cases, corresponding to a mobility ratio *M* close to 10, with a hydraulic tortuosity mean value $\langle\tau_h\rangle = 40$.

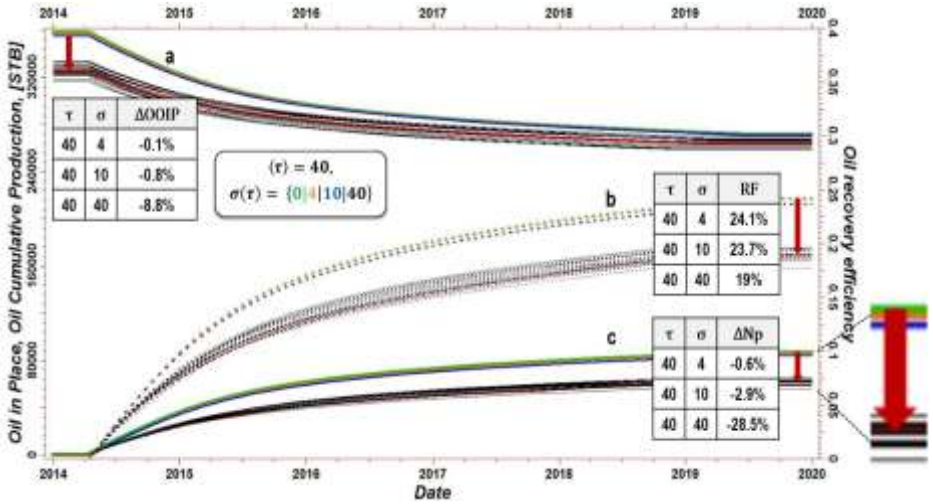


*Figure 7 - Tortuosity variability impact for the average-oil case, M ≈ 10, reservoir results*

Three sets of curves are presented in Figure 7: set (a) presents the original volume of oil in place OOIP (STB); set (b) presents the oil recovery efficiency; and set (c) presents the cumulative oil production - $N_p$ (STB).

The colors of the lines correspond to the different hydraulic tortuosity standard deviation values: green for the base case with $\sigma(\tau_h) = 0$; orange for $\sigma(\tau_h) = 4$; blue for $\sigma(\tau_h) = 10$; black for the several stochastic cases run with $\sigma(\tau_h) = 40$, and red lines corresponding to the average results.

Comparing the average-oil case with $\sigma(\tau_h) = 40$ (in red) to the base case (in green), OOIP is down by 8.8%, and ultimate oil recovery ($N_p$) is down by 28.5%. The oil recovery factor is also down from 24.1 to 19%.

On the other hand, with $\sigma(\tau) \leq 10$ (orange and blue curves), the impact on both OOIP and Np is not significant (less than 3%). The smaller the standard deviation, the better the sensitivity case matches with the base case, thus confirming the model validation.

**Figure 8** also shows the results for the average-oil cases, but for the worst-performing production well in the pattern. Only one set of curves is presented: cumulative oil production – Np (STB).

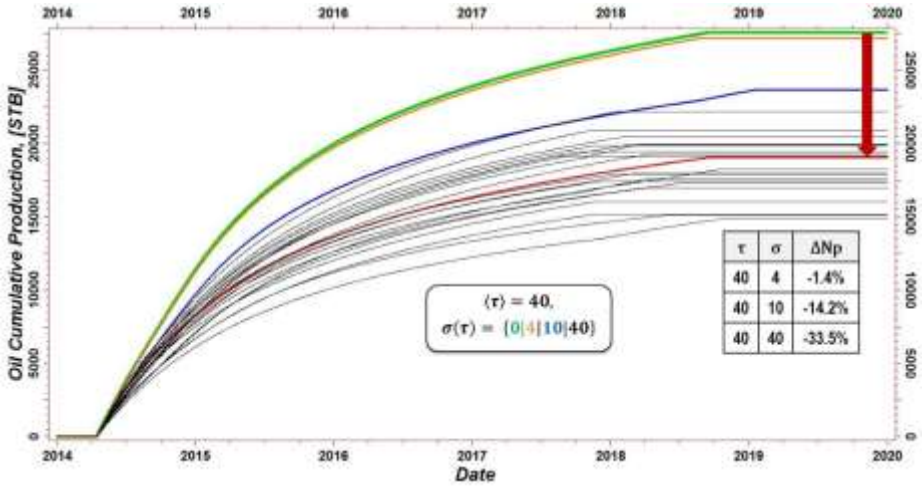


*Figure 8 - Tortuosity variability impact for the average-oil case, $M \approx 10$, worst-performing-well results. We use the same color scheme as the one in Figure 7.*

Comparing again the average-oil case with $\sigma(\tau_h) = 40$ (in red) to the base case (in green), Np is down by 33.5%. For the case with $\sigma(\tau) = 10$ (blue curve), the impact is still significant, with a 14.2% decrease in $N_p$. On the other hand, with $\sigma(\tau) \leq 4$ (orange curve), the impact is not significant, also confirming the model validation.

**Figure 9** shows the tornado charts, which summarize the sensitivity study results.

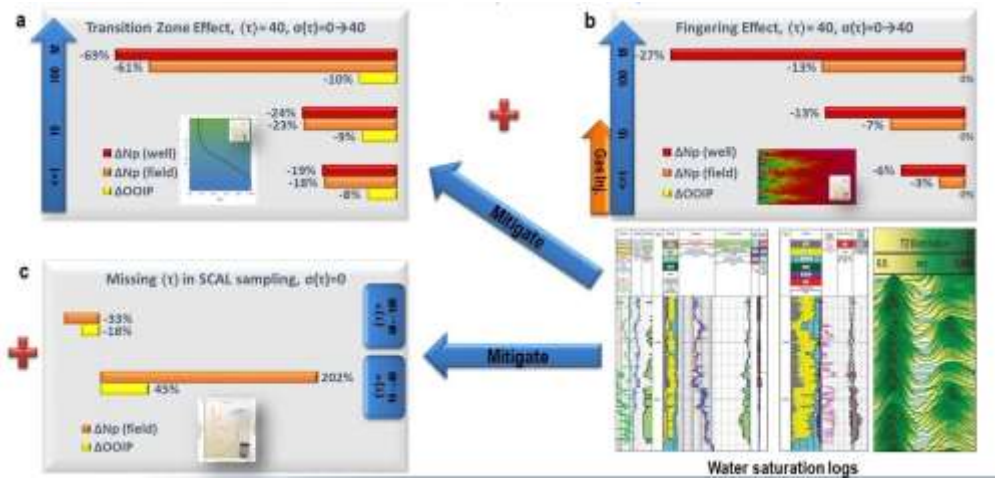


*Figure 9 - Tortuosity variability sensitivity tornado charts*

**Figure 9a** shows the impact of tortuosity variability on the oil-water transition zone, considering a mean value of $\langle \tau_h \rangle = 40$ and a standard deviation of $\sigma(\tau_h) = 40$ for the hydraulic tortuosity. It shows in yellow the impact on the reservoir OOIP; in orange the impact on the reservoir ultimate reserves; in red the impact on ultimate cumulative production from the worst-performing well. The nonlinear behavior of the capillary pressure caused by the changes in the pore-throat sizes explain such impacts through the increase of the oil-water transition zone, even though we keep the hydraulic tortuosity mean value of $\langle \tau_h \rangle = 40$ fixed. Such impacts increase as the mobility ratio (M) increases, because the heavier is the oil, the larger the base-case transition zone is. However, the impacts are all significant for all values of mobility ratio.

**Figure 9b** shows the impact of tortuosity variability on the sweep efficiency. It shows in orange the impact on the reservoir ultimate reserves and in red the impact on ultimate cumulative production from the worst-performing well. We obtain such results by artificially eliminating the transition-zone effect, preserving the OOIP and the SHM average behavior to match the base case, but keeping the same hydraulic tortuosity standard deviation of $\sigma(\tau_h) = 40$. Again, impacts are all significant, except for the light-oil cases ($M \leq 1$). Such impacts are more intense in the well's level compared with the ones at the reservoir level. The heterogeneity increase in the fluid saturation and the relative permeability end-points explains the impact of tortuosity variability on the sweep efficiency decrease.

**Figure 9c** shows the impact on OOIP and $N_p$ estimates when we unintentionally miss the mean value of the hydraulic tortuosity $\langle \tau_h \rangle$ during the SCAL sampling, particularly if the tortuosity variability is high. If no corrections are made, such experimental results are defined by the real hydraulic tortuosity of the samples. Therefore, they may not represent, for each corresponding rock type, the average capillary behavior all over the reservoir. To assess such impact, we run two additional light-oil ($M \leq 1$) sensitivity base cases, one considering a hydraulic tortuosity mean value of $\langle \tau_h \rangle = 10$ and another one with a mean value of $\langle \tau_h \rangle = 100$, both with standard deviation of $\sigma(\tau_h) = 0$. We then alternatively compare these two cases with the light-oil case with $\langle \tau_h \rangle = 40$ and $\sigma(\tau_h) = 0$. This chart shows in yellow the impact on the reservoir OOIP and in orange the impact on the reservoir ultimate reserves. When the SCAL tortuosity value ($\langle \tau_h \rangle = 40$) is greater than the actual reservoir-tortuosity mean value ($\langle \tau_h \rangle = 10$), pore-throat sizes in the SCAL samples are also greater than the actual ones (see Eq. (6)). Therefore, the oil-water transition

zone will be smaller in the reservoir simulation model than it actually is. OOIP is then severely overestimated by simulation, as well as the ultimate reserves. Conversely, when the SCAL tortuosity value ($\langle\tau_h\rangle = 40$) is smaller than the actual reservoir-tortuosity mean value ($\langle\tau_h\rangle = 100$), OOIP and $N_p$ are drastically underestimated by simulation. Therefore, we recommend applying proper corrections while deriving dynamic reservoir properties from capillary pressure and relative permeability experiments, based on the $J^*$ and $RQI^*$ concepts. We may use Eq. (15) to correct the capillary pressure results from the sample tortuosity to the reservoir-tortuosity mean value. Likewise, we may use Eq. (14) to correct the relative permeability curves parameters and corresponding end-points.

Table 3 summarizes the data shown in Figure 9.

*Table 3 - Tortuosity Variability Sensitivity Results*

| | Transition-Zone Effect | | | Fingering Effect | | | Missing $\langle\tau_h\rangle$ in SCAL | |
|---|---|---|---|---|---|---|---|---|
| $\langle\tau_h\rangle$ | 40 | | | 40 | | | 10→40 | 40←100 |
| $\sigma(\tau_h)$ | 0→40 | | | 0→40 | | | 0 | |
| M | M ≤ 1 | M = 10 | M = 100 | M ≤ 1 | M = 10 | M = 100 | M ≤ 1 | M ≤ 1 |
| ΔOOIP | -0.08 | -0.09 | -0.1 | 0 | 0 | 0 | 0.45 | -0.18 |
| $\Delta Np_{reservoir}$ | -0.18 | -0.23 | -0.61 | -0.03 | -0.07 | -0.13 | 2.02 | -0.33 |
| $\Delta Np_{well}$ | -0.19 | -0.24 | -0.69 | -0.06 | -0.13 | -0.27 | – | – |

The impacts on OOIP and $N_p$, shown in the three tornado charts, are additive, and the total impact may be positive or negative. We may mitigate the effects on the transition zone – shown in Figure 9a and Figure 9c, by artificially reconciling SCAL corrections (from laboratory to reservoir conditions) with water-saturation well logs with good quality. However, we cannot mitigate the impact on the sweep efficiency shown in Figure 9b.

Finally, we should consider which fluids are involved in the actual reservoir-energy drives. For instance, a light oil may result in favorable oil-water mobility ratios ($M \leq 1$) reducing such impacts. However, if the injected fluid is gas, it may result in less favorable mobility ratios ($M > 1$), increasing the negative impact of tortuosity variability on sweep efficiency. On the other hand, as gas is usually less dense than oil, gas injection may result in a smaller impact on the transition zone.

## Conclusions

The proposed dynamic reservoir-rock-typing index RQI* shows a much stronger correlation with pore-space geometry when compared with Winland R35, reservoir-quality (RQI) and flow-zone (FZI and FZIm) indexes. Therefore, it has clear potential to enhance the dynamic rock-typing and capillary-effects upscaling for reservoir simulation of IOR / EOR in complex carbonate rocks. The comparison between RQI* and the other indexes may further improve as the tortuosity variability of a specific dataset increases.

Hydraulic tortuosity data may be obtained from routine core analysis and standard MICP data. Likewise, electric tortuosity data may be calculated from the Archie's cementation exponent $m$, from resistivity-formation-factor experiments. Running multiple SCAL experiments on the same plugs may significantly improve the likelihood and quality of the correlations between the corresponding data.

The good correlation between hydraulic and electric tortuosity significantly increases the potential of dielectric measurements for dynamic reservoir characterization of complex carbonates on both core and

well log scales. Such correlation should be stronger for samples belonging to the same field, same formation, and same geological facies with the same clay content.

Dielectric well logs may provide cementation exponent $m$ and the corresponding electric tortuosity estimates. The combination of core and well log analysis may enable the upscaling of hydraulic tortuosity and RQI*, as well as the proper distribution of capillary pressure and relative permeability curves. The dielectric measurements may also provide good quality water-saturation estimates, which may help calibrating the reservoir saturation-height model (SHM).

To justify eventual additional SCAL experiments and well logs, the benefit corresponding to reduced uncertainty in the estimation of hydraulic tortuosity must be demonstrated. We successfully put in place a workflow for such an impact assessment through proper sensitivity analysis.

Overlooking the rock-pore-space geometry and network topology may result in significant errors in reservoir characterization and simulation processes. The sensitivity study results showed a significant impact of hydraulic tortuosity variability on oil in place and reserves estimates for IOR / EOR processes in typical complex carbonate reservoirs, such as the ones found in the Brazilian Pre-Salt.

Missing the mean value of the hydraulic tortuosity during the SCAL sampling, particularly if the tortuosity variability is high, may result in huge impacts on OOIP and ultimate reserves. Therefore, SCAL results should be corrected according to the hydraulic tortuosity value. Furthermore, such results should also be adjusted to good quality water-saturation logs in order to build a suitable reservoir SHM.

## Nomenclature

### Abbreviations

| | | |
|---|---|---|
| *API* | = | *API fluid density* |
| *BTR* | = | *pore body-to-throat-size ratio* |
| *DRRT* | = | *dynamic reservoir-rock typing* |
| *EOR* | = | *enhanced oil recovery* |
| *FZI* | = | *flow-zone indicator* |
| $FZI_m$ | = | *Nooruddin et al. (2011) modified flow zone indicator* |
| *FWL* | = | *free-water level for reservoir capillary pressure reference* |
| *HFU* | = | *hydraulic flow units* |
| *IOR* | = | *improved oil recovery* |
| *K-C* | = | *Kozeny-Carman* |
| *MICP* | = | *mercury-injection capillary pressure* |
| *NMR* | = | *nuclear magnetic resonance* |
| *OOIP* | = | *original volume of oil in place* |
| *Np* | = | *cumulative oil production* |
| *RFF* | = | *resistivity-formation factor* |
| *RQI* | = | *reservoir-quality index* |
| *RQI** | = | *proposed dynamic reservoir-rock-typing index* |
| *SCAL* | = | *special core analysis* |
| *SGS* | = | *sequential Gaussian simulation* |
| *SHM* | = | *saturation height model* |
| *WAG* | = | *water-alternating-gas injection* |
| *WWRC* | = | *joint-industry worldwide rock catalog* |

## Symbols

| | | |
|---|---|---|
| $k$ | = | *absolute permeability* |
| $\phi_e$ | = | *effective porosity* |
| $\phi_z$ | = | *normalized porosity* |
| $R_{35}$ | = | *pore-throat radius corresponding to the capillary pressure at 35% of mercury saturation* |
| $P_c$ | = | *capillary pressure* |
| $\gamma$ | = | *fluids' interfacial tension* |
| $\theta$ | = | *rock-fluids-contact angle* |
| $r_{throat}$ | = | *pore-throat radius* |
| $\tau_h$ | = | *hydraulic tortuosity* |
| $f_g$ | = | *Kozeny-Carman shape factor* |
| $\tau_{kc}$ | = | *Kozeny-Carman tortuosity* |
| $S_{Vgr}$ | = | *specific surface area of a grain* |
| $\tau_e$ | = | *electric tortuosity* |
| $\phi$ | = | *total porosity* |
| $S_w$ | = | *wetting-fluid saturation (air for MICP, water for RFF)* |
| $S_{wmin}$ | = | *minimum wetting-fluid saturation* |
| $S_w^*$ | = | *normalized wetting-fluid saturation* |
| $S_{Hg}$ | = | *mercury (non-wetting-fluid) saturation* |
| $a$ | = | *Archie's tortuosity factor* |
| $m$ | = | *Archie's cementation exponent* |
| $n$ | = | *Archie's saturation exponent* |
| $J^*$ | = | *El-Khatib (1995) modified Leverett* |
| $J$ | = | *Leverett J-function* |
| $k^*$ | = | *modified absolute permeability* |
| $T_M$ | = | *simulation transmissibility multiplier* |
| $T_M^*$ | = | *modified transmissibility multiplier* |
| $\sigma$ | = | *standard deviation* |
| $M$ | = | *mobility ratio between the displacing and displaced fluids* |
| $P_{sat}$ | = | *pressure at saturation point* |
| $B_{oi}$ | = | *oil formation volume factor* |
| $\mu_{oi}$ | = | *oil viscosity* |
| $R_{si}$ | = | *dissolved gas-oil ratio* |
| $R_d$ | = | *pore-throat size corresponding to the entry capillary pressure* |

## Conversion Factors

All equations are presented considering the use of a consistent unit system. If a field-unit system is used then proper conversion factors should be applied.

## Acknowledgements

The authors would like to acknowledge the Schlumberger Brazil Research and Geoengineering Center management, petrophysics and reservoir engineering program teams.

## References


Al-Kharusi, A.S., Blunt, M.J., 2007. Network Extraction from Sandstone and Carbonate Pore Space Images. Journal of Petroleum Science and Engineering 56-4, 219 – 231.http://dx.doi.org/10.1016/j.petrol.2006.09.003

Amaefule, J. O., Altunbay, M., Tiab, D., Kersey, D. G., & Keelan, D. K., 1993. Enhanced Reservoir Description: Using Core and Log Data to Identify Hydraulic (Flow) Units and Predict Permeability in Uncored Intervals/Wells. Presented at SPE Annual Technical Conference and Exhibition, 3-6 October, Houston, Texas. SPE-26436-MS. http://dx.doi.org/10.2118/26436-MS.

Arns, J.-Y. and Robins, V. and Sheppard, A.P. and Sok, R.M. and Pinczewski, W.V. and Knackstedt, M.A., 2004. Effect of Network Topology on Relative Permeability. Transport in Porous Media 55-1, 21–46. http://dx.doi.org/10.1023/B:TIPM.0000007252.68488.43

Bize-Forest, N., Baines, V., Boyd A., Moss A., Oliveira R., 2014. Carbonate Reservoir Rock Typing and the Link between Routine Core Analysis and Special Core Analysis. Presented at the International Symposium of the Society of Core Analysts, 8-11 September, Avignon, France, SCA2014-A057

Buiting, J.J.M. and Clerke, E.A., 2013. Permeability from Porosimetry Measurements: Derivation for a Tortuous and Fractal Tubular Bundle. Journal of Petroleum Science and Engineering 108, 267–278. http://dx.doi.org/10.1016/j.petrol.2013.04.016

Clennell, M.B., 1997. Tortuosity: a Guide through the Maze. Geological Society Special Publication 122, 299–344. http://dx.doi.org/10.1144/GSL.SP.1997.122.01.18

Clerke, E.A. and Mueller III, H.W. and Phillips, E.C. and Eyvazzadeh, R.Y. and Jones, D.H. and Ramamoorthy, R. and Srivastava, A., 2008. Application of Thomeer Hyperbolas to Decode the Pore Systems, Facies and Reservoir Properties of the Upper Jurassic Arab D Limestone, Ghawar Field, Saudi Arabia: A "Rosetta Stone" Approach. GeoArabia 13-4, 113–160.

Core Lab, 2014. Worldwide Rock Catalog™, http://www.corelab.com/irs/studies/wwrc (accessed 19th of June 2015)

Cosentino, L., 1992. Integrated Reservoir Studies. Editions Technip, Paris.

Dullien, F. A. L., 1979. Porous Media: Fluid Transport and Pore Structure. Academic Press, San Diego.

El-Khatib, N., 1995. Development of a Modified Capillary Pressure J-function. Presented at SPE Middle East Oil Show, 11-14 March, Bahrain, SPE-29890-MS. http://dx.doi.org/10.2118/29890-MS

Haro, C.F., 2007. Permeability Modeling. Setting Archie and Carman-Kozeny Right. Presented at SPE International Oil Conference and Exhibition in Mexico, 27-30 June, Veracruz, Mexico, SPE-100201-MS. http://dx.doi.org/10.2118/100201-MS

Jerry Lucia, F., 1999. Characterization of Petrophysical Flow Units in Carbonate Reservoirs: Discussion. AAPG Bulletin 83-7, 1161–1163.

Kenyon, W. E., Allen, D. F., Lisitza, N. V., & Song, Y. Q., 2002. Better Pore-Size Distributions from Stimulated-Echo NMR Lab Measurements Using Magnetic Susceptibility Contrast and Small Encoding Angles. SPWLA Symposium Transactions, SPWLA-2002-III.

Kleinberg, R. L., & Vinegar, H. J., 1996. NMR Properties of Reservoir Fluids, SPWLA, The Log Analyst, 37-6, 20-32

Klinkenberg, L.J., 1941. The Permeability of Porous Media to Liquids and Gases. American Petroleum Institute, API-41-200.

Kozeny, J., 1927. Uber die Kapillare Leitung Deswassers im Boden (Aufstieg Versickerung und Anwendung auf die Bewasserung. Sitz. Ber. Akad. Wiss,Wien, Math. Nat. (Abt. Iia) 136a, 271.

Leverett, M., 1941. Capillary Behavior in Porous Solids. SPE Trans. AIME 42-1, 152–169. SPE-941152-G. http://dx.doi.org/10.2118/941152-G

Lindquist, W.B. and Venkatarangan, A. and Dunsmuir, J. and Wong, T.-F., 2000. Pore and Throat Size Distributions Measured from Synchrotron X-ray Tomographic Images of Fontainebleau Sandstones. Journal of Geophysical Research: Solid Earth 105-89, 21509–21527.

Nooruddin, H., Hossain, M. E., Sudirman, S. B., & Sulaimani, T., 2011. Field Application of a Modified Kozeny-Carmen Correlation to Characterize Hydraulic Flow Units. Presented at SPE/DGS Saudi Arabia Section Technical Symposium and Exhibition, 15-18 May, Al-Khobar, Saudi Arabia. SPE-149047-MS. http://dx.doi.org/10.2118/149047-MS

Øren, P.E., Bakke, S., 2003. Reconstruction of Berea Sandstone and Pore-Scale Modelling of Wettability Effects. Journal of Petroleum Science and Engineering 39-3/4, 177 – 199. http://dx.doi.org/10.1016/S0920-4105(03)00062-7

Pizarro, J. O. D. S., & Branco, C. C. M., 2012. Challenges in Implementing an EOR Project in the Pre-Salt Province in Deep Offshore Brasi. Presented at SPE EOR Conference at Oil and Gas West Asia, 16-18 April, Muscat, Oman. SPE-155665-MS. http://dx.doi.org/10.2118/155665-MS

Seleznev, N., Boyd, A., Habashy, T., & Luthi, S. M., 2004. Dielectric Mixing Laws for Fully and Partially Saturated Carbonate Rocks. Presented at SPWLA 45th Annual Logging Symposium, 6-9 June, Noordwijk, Netherlands. SPWLA-2004-CCC

Seleznev, N. V., Habashy, T. M., Boyd, A. J., & Hizem, M., 2006. Formation Properties Derived from a Multi-Frequency Dielectric Measurement. Presented at SPWLA 47th Annual Logging Symposium, 4-7 June, Veracruz, Mexico. SPWLA-2006-VVV

# Appendix A: Tortuosity, $J^*$-Function and RQI versus FZI Discussion

## Tortuosity Definition

Clennell (1997) presented a comprehensive literature review on the several tortuosity concepts and definitions: "Tortuosity can have various meanings when used by physicists, engineers or geologists to describe different transport processes taking place in a porous material. Values for geometrical, electrical, diffusional and hydraulic tortuosity are in general different from one another." In this study, we keep Clennell's (1997) definition for tortuosity: "Tortuosity can be redefined in terms of the energetic efficiency of a flow process. The efficiency is related to the rate of entropy dissipation (or isothermally, energy dissipation) with respect to a simple, non-tortuous model medium using the postulates of non-equilibrium thermodynamics."

The simplest hydraulic tortuosity concept is defined using a circular-tube-bundle rock model as shown below in **Figure A.1b**, where all tubes are isolated from each other and have the same constant radius and the same tortuous path length $L_e$ (**Figure A.1a)**. The hydraulic tortuosity $\tau_h$ is then described as the ratio between the actual and the ideal absolute permeability $k$ based on the effective porosity $\phi_e$ and the radius $R$ of the tubes, by making the viscous-fluid-laminar-flow assumption.

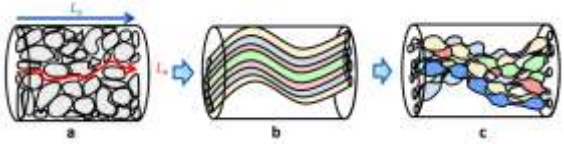


*Figure A.1 – Rock-pore-space models: tortuous path (a), simple tube bundle (b) and complex tube bundle (c)*

The hydraulic tortuosity $\tau_h$ is given by the Kozeny (1927) equation:

$$k = \frac{\phi_e R^2}{8\,\tau_h}, \tag{A.1}$$

and calculated by:

$$\tau_h = \tau_g = \frac{L_e^2}{L_s^2}, \tag{A.2}$$

where $L_e$ is the tube tortuous length and $L_s$ is the straight core-plug length as illustrated in Figure A.1(a). The tortuosity defined by Eq. (A.2) only includes a basic geometric concept of tortuosity $\tau_g$.

Such bundle-of-tubes model has many limiting assumptions: constant tube circular radius, constant tortuous path length, and no connectivity between tubes. The actual rock-pore space consists of interconnected pore throats and pore bodies of different sizes and geometries as shown in **Figure A.1c**. The pore-space-size distribution, its geometry type, the pore-body-to-pore-throat-size aspect ratio (*BTR*)

and the degree of pore-network connectivity (given by the coordination number $Z_c$) influence the energetic efficiency of the hydraulic flow process, depending on the rock genesis, compaction and diagenesis history. Besides the rock-pore-space complexity, such efficiency may also be affected by local turbulence in sudden changes of pore size and flow direction; non-Darcy flow; saturation fluids; thin film of wetting fluids; clay swelling and low-density-gas slippage.

We present the following definition for hydraulic tortuosity, consistent with the energetic efficiency approach mentioned above:

$$\tau_h = \frac{\phi_e \langle r_{\text{throat}}^2 \rangle}{8k}, \tag{A.3}$$

where $\langle r_{\text{throat}}^2 \rangle$ is the average pore-throat squared radius obtained from a mercury-injection-capillary-pressure (MICP) experiment. The proposed definition is very practical as MICP experiments are widely available in the industry. MICP is also consistent with conventional core analysis for determination of $\phi_e$ and $k$, as both are run under similar wettability conditions, having gas as the wetting phase. Usual corrections for rock compressibility and gas slippage (Klinkenberg, 1941) should be applied.

MICP and gas effective porosity are both volumetric (3D) experiments. Nevertheless, absolute permeability experiments are essentially unidirectional. Therefore, the hydraulic tortuosity defined by Eq. (A.3) presents the same degree of anisotropy of the absolute permeability property. Besides, under such directional constrain, a certain fraction of the so-called tubes does not connect from the inlet to the outlet of the core plug, contributing to the effective porosity and pore-throat distribution, but not to the permeability in the corresponding direction. In this study, we also analyze electric tortuosity $\tau_e$ data from resistivity-formation-factor (RFF) experiments.

We use the electric tortuosity definition presented by both Clennell (1997) and Nooruddin et al. (2011), represented by the equation:

$$\tau_e = \left(\frac{a}{\phi^{(m-1)}}\right)^2, \tag{A.4}$$

where $\phi$ is the total porosity, $a$ is the tortuosity factor and $m$ is the cementation exponent from the Archie's semi-empirical equation.

The energetic efficiency approach to tortuosity determination compares actual measurements from standard experiments with ideal results from base porous-media models. Therefore, it is important to keep consistency between such base models and the tortuosity-related models used in the well log and reservoir scales.

These hydraulic and electric-tortuosity models are quite simple. We believe they have significant potential for improvement by including additional rock-pore-space properties and transport-phenomena aspects. Such improved models may enhance the correlation between hydraulic and electric tortuosity and other rock properties, but they may require new measurements in both core and well log scales.

## El-Khatib $J^*$-Function

El-Khatib (1995) presented a modified $J$-function as an improvement to the Leverett $J$-function, incorporating the hydraulic tortuosity $\tau_h$ and irreducible water saturation $S_{wirr}$ data, defined by:

$$J^*(S_w^*) = \frac{P_c}{\gamma \cos(\theta)} \sqrt{\frac{k\tau_h}{\phi_e(1 - S_{wirr})}}, \tag{A.5}$$

where $P_c$ is the drainage capillary pressure, $\gamma$ is the fluids' interfacial tension, $\theta$ is the fluid-rock contact angle and where the normalized water saturation $S_{\mathrm{w}}^*$ is defined by:

$$S_{\mathrm{w}}^* = \frac{(1 - S_{\mathrm{w}})}{(1 - S_{\mathrm{wirr}})}. \tag{A.6}$$

In his formulation, El-Khatib (1995) used an integral form of Eq. (A.3):

$$\tau_h = \frac{\phi_e}{8k} \int_{S_{wirr}}^{1} r_{\mathrm{throat}}^2 . dS_{\mathrm{w}}\,, \tag{A.7}$$

giving rise to the term $(1 - S_{wirr})$ in Eq. (A.5). Instead, if the integral in Eq. (A.7) is defined from 0 to 1 over the normalized saturation differential $dS_w^*$, Eq. (A.7) is then fully consistent with $\langle r_{\mathrm{throat}}^2 \rangle$ in Eq. (A.3) and the truncation term $(1 - S_{wirr})$ is not anymore required. The corrected El-Khatib $J$-function equation becomes:

$$J^*(S_w^*) = \frac{P_c}{\gamma \cos(\theta)} \sqrt{\frac{k\tau_h}{\phi_e}} = \frac{2}{r_{\mathrm{throat}}} \sqrt{\frac{k\tau_h}{\phi_e}} = \sqrt{\frac{\langle r_{\mathrm{throat}}^2 \rangle}{2r_{\mathrm{throat}}^2}}. \tag{A.8}$$

## Comparison between RQI and FZI indexes

To understand the differences between RQI and FZI concepts, we compare the corresponding modified Kozeny Eq. (A.1) with the Kozeny -Carman equation:

$$k = \left( \frac{1}{f_g \tau_{kc} S_{Vgr}^2} \right) \phi_e \, \phi_z^2, \tag{A.9}$$

where $f_g$ is the shape factor, $\tau_{kc}$ is the K-C tortuosity, $S_{Vgr}$ is the specific surface area of the grain and $\phi_z$ is the normalized porosity (Amaefule et. al., 1993). These equations were derived from different perspectives: while Kozeny dimension corresponds to the pore size, Carman dimension corresponds to the grain size. For both Eqs. (A.1) and (A.9) to give the same resulting $k$ as a function of $\phi_e$, we require:

$$\tau_h = \frac{f_g \tau_{kc}}{8\phi_z^2} \, S_{Vgr}^2 R^2 \,. \tag{A.10}$$

From Eq. (A.10), $\tau_h$ and $\tau_{kc}$ clearly represent different principles. Moreover, the product $S_{Vgr}^2 R^2$ is dimensionless. Therefore, for simple pore-space models, Eq. (A.10) should be further simplified. In the case of the circular-tube-bundle rock model shown in Figure A.1b we get:

$$S_{vgr} = \frac{S_{gr}}{V_{gr}} = \frac{2\pi nRL_e}{\frac{(1-\phi_e)}{\phi_e}.V_{pore}} = \phi_z \cdot \frac{2\pi nRL_e}{\pi nR^2 L_e} = \phi_z \cdot \frac{2}{R}, \quad \text{(A.11)}$$

where $n$ is the number of tubes. Substitution of Eq. (A.11) in Eq. (A.10) gives:

$$\tau_h = {}^{f_g \tau_{kc}}/_{2}. \quad \text{(A.12)}$$

In the case of a same-size-spherical-grain-pack model, we get:

$$S_{vgr} = \frac{S_{gr}}{V_{gr}} = \frac{4\pi nrR_{gr}^2}{4/3\,\pi nR_{gr}^3} = \frac{3}{R_{gr}} = \frac{3}{\omega R}, \quad \text{(A.13)}$$

where $R_{gr}$ is the grain radius and $\omega$ is the ratio between $R_{gr}$ and the equivalent pore radius $R$. The ratio $\omega$ is constant for each specific sphere-packing geometry. Therefore, substitution of Eq. (A.13) in Eq. (A.10) gives:

$$\tau_h = \frac{9 f_g \tau_{kc}}{8\omega^2 \phi_z^2}. \quad \text{(A.14)}$$

By examining Eq. (A.14), it is clear that the normalized porosity $\phi_z$ partially accounts for the hydraulic tortuosity $\tau_h$, in the case of rocks with round-shaped grains with low to moderate diagenesis. Nevertheless, examining Eq. (A.12), the normalized porosity $\phi_z$ term is cancelled out and does not account for the hydraulic tortuosity $\tau_h$ in the case of cylindrical pores.

The RQI equation considers an implicit constant hydraulic tortuosity $\tau_h$. Therefore, we conclude that the FZI formulation is superior to the RQI formulation in the case of rocks with round-shaped grains with low to moderate diagenesis, while RQI is preferred in the case of cylindrical pores resulting from intense diagenesis.

Having such ideal cases in mind, when dealing with real rock types, we recommend analyzing the correlations of both FZI and RQI with other rock properties and hydraulic flow units (HFU), and choosing the index with better results. However, if tortuosity data is available, we recommend using our proposed RQI* index over, or in addition to the FZI or RQI indexes.